



Experimental and modeling study on water dynamic transport of the proton exchange membrane fuel cell under transient air flow and load change

Shuguo Qu^{a,b}, Xiaojin Li^{a,*}, Changchun Ke^{a,b}, Zhi-Gang Shao^a, Baolian Yi^a

^a Fuel Cell System and Engineering Laboratory, Dalian Institute of Chemical Physics, Chinese Academy of Sciences, No. 457 Zhongshan Rd., Dalian 116023, PR China

^b Graduate University of Chinese Academy of Sciences, Beijing 100039, PR China

ARTICLE INFO

Article history:

Received 6 April 2010

Accepted 9 April 2010

Available online 6 May 2010

Keywords:

Proton exchange membrane fuel cell

Transient response

Water transport

Transient air flow change

Load change

ABSTRACT

Water management is important in the proton exchange membrane fuel cell (PEMFC) operations, especially for those cells based on sulfonic acid polymers due to the depending of the conductivity on water. This paper aims at illustrating the effect of the change in membrane water content on cell potential response. For this purpose, the cell potential response has been investigated experimentally and computationally under transient air flow and load change of a PEMFC. From the experimental and computational results, an undershoot behavior of cell potential as well as the great influence of the relative humidity on the magnitude of undershoot is observed. It is found that the magnitude of cell potential undershoot increases as the relative humidity decreases. By carrying out a transient simulation on the water content of the membrane, the undershoot phenomena could be well explained. It is also found from the computational prediction that the time scale for the cell potential to reach its steady state is about 20 s, in agreement with experimental results. The model prediction also suggests that the dynamic behavior of PEMFC is critically dependent on the water content in the membrane.

Crown Copyright © 2010 Published by Elsevier B.V. All rights reserved.

1. Introduction

The proton exchange membrane fuel cell (PEMFC) is regarded as a potential power source in the future for electrical vehicles, due to its high efficiency, zero emission and fast start-up at room temperature. However, there are still many critical issues that need to be improved before PEMFC can be commercially produced. One of the most important problems is water management during the PEMFC operation. It is well known that the performance of PEMFC depends strongly on the water balance within the fuel cell. At a low humidity, the membrane electrode assembly (MEA) adherent to anode side will lose water, thus leading to a rapid increase in the ohmic resistance [1]. On the contrary, if too much liquid water exists in the cell, the catalytic active sites will be covered and oxygen transport will be obstructed in the cathode gas diffusion electrode. Therefore, a sophisticated water balance in the PEMFC must be maintained to avoid membrane dehydration and cathode flooding.

In the past decades, numerous studies on water transport in the PEMFC have been conducted. Many experimental studies have been devoted to the describing of the water transport behavior in the

PEMFC [2–6]. Springer et al. [2] have obtained correlations for water diffusion coefficient and electro-osmotic drag coefficient based on ex situ measurements. Zawodzinski et al. [3] have studied water transport in Nafion 117 membrane at 30 °C. Hinatsu et al. [4] have also performed an experiment to investigate the water uptake process, and observed the performance of the membrane submerged in the liquid water at the temperatures from 25 to 130 °C. Janssen and Overvelde [5] have presented measured results of the net drag coefficient for Nafion 112 membrane using a condenser connected to the cell outlets to collect water. Husar et al. [6] have studied three different mechanisms of water transport in an operating PEMFC under specially imposed boundary conditions and obtained in situ results of water transfer due to different mechanisms. These experimental results not only could supply the empirical correlations which could be adopted in model calculations, but also could verify the effectiveness of the model. In addition to experimental investigations, most studies on water transport within fuel cells were based on mathematical model [7–18]. Bernardi and Verbrugge [7] have put forward a model to describe the water transport in the proton exchange membrane (PEM) and cathode CL. Springer et al. [2] have proposed a one-dimensional isothermal model to analyze the water transport, and found that the net-water-per-proton flux ratio was much less than the measured electro-osmotic drag coefficient for a fully hydrated membrane. The Okada group has concentrated their studies on water transport and distribution in the electrolyte membrane of the PEMFC to investigate the influ-

* Corresponding author. Tel.: +86 411 84379051; fax: +86 411 84379185.

E-mail addresses: qushg05@dicp.ac.cn (S. Qu), xjli@dicp.ac.cn (X. Li), kechangchun@dicp.ac.cn (C. Ke), zhgshao@dicp.ac.cn (Z.-G. Shao), bllyi@dicp.ac.cn (B. Yi).

Nomenclature

a_k	activity of water in stream k , dimensionless
c	molar concentration of species, mol m^{-3}
D	diffusion coefficients, $\text{m}^2 \text{s}^{-1}$
V_{cell}	cell operating potential, V
V_{oc}	open-circuit voltage, V
F	Faraday's constant, 96487 C mol^{-1} ; body force
I	cell operating current density, A m^{-2}
i_a	anode local current density, A m^{-2}
i_c	cathode local current density, A m^{-2}
$i_{o,a}^{\text{ref}}$	anode reference exchange current density, A m^{-2}
$i_{o,c}^{\text{ref}}$	cathode reference exchange current density, A m^{-2}
k_p	hydraulic permeability, m^2
M_{O_2}	molecular weight of oxygen, kg mol^{-1}
M_{H_2}	molecular weight of hydrogen, kg mol^{-1}
$M_{\text{H}_2\text{O}}$	molecular weight of water, kg mol^{-1}
n_d	electro-osmotic drag coefficient
p	pressure, atm
R	universal gas constant, $8.314 \text{ J mol}^{-1} \text{ K}^{-1}$
S	source
T	temperature, K
t_m	thickness of the membrane, m
u	velocity vector, m s^{-1}
α	total water drag from the anode to cathode, dimensionless
λ	membrane water content
ε	porosity
η	overpotential, V
μ	viscosity, $\text{kg m}^{-1} \text{ s}^{-1}$
ρ	density, kg m^{-3}
σ_m	membrane electronic conductivity, S m^{-1}
Φ_s	electrode potential, V
Φ_e	membrane potential, V
t_m	membrane thickness, m

ence of the membrane characteristics, operating conditions, and contamination effects [9–12].

However, those aforementioned works were done mainly on steady state analysis; studies on membrane water content dynamic transport were rare. Chen et al. [13] have found that the membrane swelling effect would increase the membrane water content, especially in the region close to the membrane/cathode interface, thus lengthening the response time for a PEMFC to attain steady state, in comparing with the case ignoring this effect. Wang and Wang [17] have performed numerical simulations for a single channel PEMFC undergoing a step increase in current density. Their results elucidated impressive interactions between the cell voltage response and the water transport dynamics in a low-humidity PEMFC. However, they had not considered the effect of current density on the membrane water content under variable flow rates. Wu et al. [18] have studied the membrane hydration/dehydration processes during the step increase in cell voltage under a constant flow rate. It is worth pointing out that all the predictions except in Refs. [19,20] employed a constant flow rate during load change to study the transient behavior of the PEMFC. Hu and Fan [19] have taken into account the effect of a variable flow rate on the dynamic behavior by adopting a sinusoidal change of air stoichiometry while keeping other parameters constant. Our group [20] has studied the air stoichiometry change rate and pattern, as well as its lagging time to load change and the initial value on the dynamic behavior of a PEMFC. However, to our knowledge, no work has been done yet to study the effect of membrane water content on the cell poten-

tial by applying a variable flow rate during load change of the PEMFC.

Therefore, the objective of this study is to illustrate the effect of membrane water content on the PEMFC performance corresponding to current density change under a variable cathode flow rate through both experimental and modeling methods. Firstly, charge conservation equations were added to our previous work [20] to study the PEMFC potential transient responses during both the cathode flow rate change and the load change processes. Then, a specially designed test cell was used to measure the cell potential responses to the variable cathode flow rate during load change in the PEMFC. Finally, the predicted cell potential transient responses through model calculation were compared with the experiment results and the effect of membrane water content change on cell potential during transient air flow and load change of PEMFC was analyzed.

2. Mathematic model

2.1. Model assumptions

In the present work, the assumptions and simplifications adopted in the model are as follows:

- (1) The cell operates under isothermal conditions at 60°C .
- (2) The gas mixture is an incompressible ideal fluid.
- (3) The flow in the gas channel is laminar.
- (4) Channels in the experimental test cell have the same geometry and same surface roughness. The diffusion layer, catalyst layer and membrane are isotropic and homogeneous, and the membrane is impermeable to gas species.
- (5) Ohmic potential drops in the diffusion layers and bipolar plates are negligible due to their high electrical conductivities.
- (6) The contact resistance between any two parts in the fuel cell is neglected.
- (7) The catalyst layer is considered as a thin interface between the proton exchange membrane and the gas diffusion electrode.
- (8) It is considered that water exits in the gas phase at the electrodes as well as in the liquid phase within the membrane. In channels, existence of liquid water is in a small volume fraction and in finely dispersed droplets so that it does not affect the gas flow.

2.2. Computational domain

The physical model is schematically shown in Fig. 1, including both the anode and cathode reaction sides and their respective flow channels separated by the MEA.

2.3. Governing equations

Generally speaking, fuel cell operation under isothermal conditions is described by mass, momentum, species, electron and proton conservation principles. Thus, under the above-mentioned assumptions, the governing equations can be written as:

Continuity:

$$\frac{\partial \rho}{\partial t} + \nabla \cdot (\rho u) = S_m \quad (1)$$

Momentum:

$$\frac{1}{\varepsilon} \left[\frac{\partial (\rho u)}{\partial t} + \frac{1}{\varepsilon} \nabla \cdot (\rho u u) \right] = -\nabla p + \nabla \cdot \tau + S_u \quad (2)$$

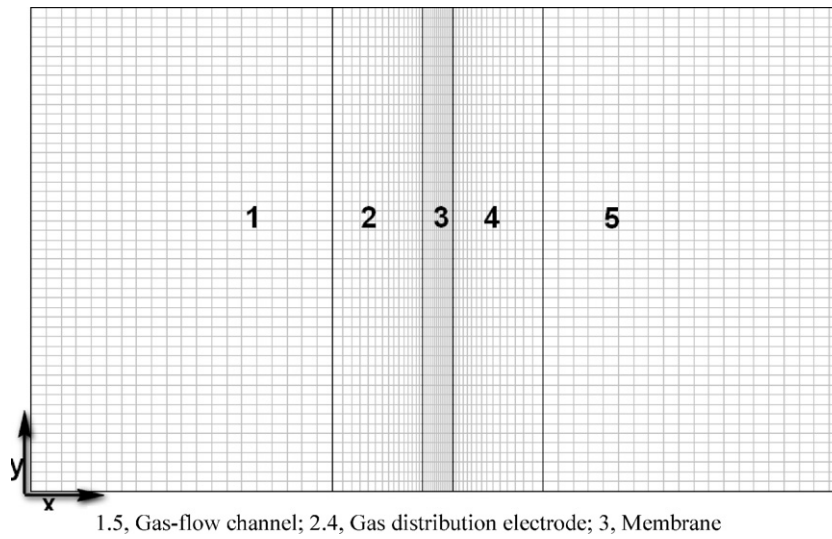


Fig. 1. Two-dimensional mesh of the PEM fuel cell in modeling geometry.

Table 1

Source terms for governing equations in various regions of a PEMFC.

	GDL	CL, a	CL, c	Membrane
Mass	$S_m = 0$	$S_m = M_{H_2} S_{H_2} + M_{H_2O} S_W^a$	$S_m = M_{H_2O} S_{O_2} + M_{H_2O} S_W^c$	$S_m = 0$
Momentum	$S_u = -\frac{\mu}{k_p} \bar{u}$	$S_u = -\frac{\mu}{k_p} \bar{u}$	$S_u = -\frac{\mu}{k_p} \bar{u}$	/
Species	$S_{H_2} = 0$	$S_{H_2} = -i_a/2F$	$S_{H_2} = 0$	$S_{H_2} = 0$
	$S_{O_2} = 0$	$S_{O_2} = 0$	$S_{O_2} = -i_c/4F$	$S_{O_2} = 0$
	$S_w = 0$	$S_w^a = -\frac{n_d}{F} i_a$	$S_w^c = \frac{n_d}{F} i_c + \frac{i_c}{2F}$	$S_w = 0$
Electron	/	$S_s = -i_a$	$S_s = i_c$	/
Proton	/	$S_e = i_a$	$S_e = -i_c$	/

Species:

$$\frac{\partial c_k}{\partial t} + \nabla \cdot (uc_k) = \nabla \cdot (D_k^{eff} \nabla c_k) + S_k \quad (3)$$

Electron transport:

$$-\nabla \cdot (\sigma_s \nabla \Phi_s) = S_s \quad (4)$$

Proton transport:

$$-\nabla \cdot (\sigma_e \nabla \Phi_e) = S_e \quad (5)$$

Source terms in the above governing equations are summarized in Table 1 for various sub-domains of the PEMFC. In the gas channels, the porosity ε becomes unity, and Eq. (2) becomes the conventional form of the momentum equation. In the porous media region, the source term in momentum conservation equation, S_u , represents Darcy's drag force. At the catalyst reactive boundary, the Butler–Volmer kinetic equation [21] is used to obtain the source term of Eqs. (4) and (5):

Anode:

$$i_a = ai_{0,a} \left(\frac{c_{H_2}}{c_{H_2,ref}} \right)^{1/2} \left(\exp \left(\frac{\partial_a^c F}{RT} \eta_a \right) - \exp \left(\frac{\partial_a^c F}{RT} \eta_a \right) \right) \quad (6)$$

Cathode:

$$i_c = ai_{0,c} \left(\frac{c_{O_2}}{c_{O_2,ref}} \right) \left(\exp \left(\frac{\partial_c^c F}{RT} \eta_c \right) - \exp \left(\frac{\partial_c^c F}{RT} \eta_c \right) \right) \quad (7)$$

where a_a^c , a_c^c , a_a^c and a_c^c are the anodic and cathodic charge transfer coefficient, η_a and η_c the anodic and cathodic local activation overpotential. For the anode reaction, the activation overpotential is the difference between the electrode and the membrane phase potentials, and the open-circuit potential of the anode is based on the standard hydrogen electrode:

$$\eta_a = \Phi_s - \Phi_e \quad (8)$$

For the cathode reaction, the activation overpotential is defined as:

$$\eta_c = \Phi_s - \Phi_e - V_{oc} \quad (9)$$

Where V_{oc} is the thermodynamic open-circuit potential for the overall reaction and is calculated using the Nernst law [21]

$$V_{oc} = 1.229 - 8.5 \times 10^{-4}(T - 298.15) + 4.308 \times 10^{-5} T (\ln(P_{H_2}^*) + 0.5 \ln(P_{O_2}^*)) \quad (10)$$

This reduces to [22] as has been done by previous researchers [23].

$$V_{oc} = 0.2329 + 0.0025T \quad (11)$$

The proton conductivity in the membrane phase has been correlated by Springer et al. [2] in 1991 as

$$\sigma_m = (0.5139\lambda - 0.326) \exp \left[1268 \left(\frac{1}{303} - \frac{1}{T} \right) \right] \quad (12)$$

where the water content in the membrane, λ , depends on the water activity, a_k , according to the following fitting of the experimental

data

$$\begin{aligned}\lambda &= 0.043 + 17.81a_k - 39.85a_k^2 + 36.0a_k^3; 0 < a_k \leq 1 \\ \lambda &= 14 + 1.4(a_k - 1); 1 \leq a_k \leq 3 \\ \lambda &= 16.8; a_k \geq 3\end{aligned}\quad (13)$$

In the past decade, several related models have been proposed to describe membrane conductivity subsequently [24–26]. However, those models were quite complicated and the physical parameters in the models were difficult to be determined. On the other hand, the membrane conductivity given by Springer et al. was expressed in water content and temperature in a simple formula, and these two parameters in the formula could be easily determined. So this model has been widely accepted and used in most of the numerical studies on the PEMFC.

Once the electrode phase potential is determined at the cathode/membrane catalyst reactive interface, the fuel cell potential can be determined by

$$V_{\text{cell}} = \frac{1}{L_{\text{ch}}} \int_0^{L_{\text{ch}}} \Phi_s dy \quad (14)$$

2.4. Boundary conditions

2.4.1. Inlet boundaries

Inlet values at the anode and cathode flow channels are prescribed for the velocity and species mass fraction (Dirichlet conditions). At the gas channel inlet, the inlet velocity u_{in} is expressed by the respective reactant stoichiometric flow ratio of the anode and cathode, ξ_a and ξ_c , defined on the basis of the desired operating current density, I_{ref} , as follows:

$$u_{a,\text{in}} = \zeta_a \frac{I_{\text{ref}}}{2F} \frac{1}{X_{\text{H}_2,\text{in}}} \frac{RT_{a,\text{in}}}{P_{a,\text{in}}} \frac{A_m}{A_{\text{ch}}} \quad (15)$$

$$u_{c,\text{in}} = \zeta_c \frac{I_{\text{ref}}}{4F} \frac{1}{X_{\text{O}_2,\text{in}}} \frac{RT_{c,\text{in}}}{P_{c,\text{in}}} \frac{A_m}{A_{\text{ch}}} \quad (16)$$

where A_m is the geometrical area of the membrane and A_{ch} the cross-sectional area of the gas channel. $X_{\text{H}_2,\text{in}}$ is the molar fraction of hydrogen and $X_{\text{O}_2,\text{in}}$ the molar fraction of oxygen at the gas channel inlet.

2.4.2. Outlet boundaries

For the outlets, the corresponding boundary conditions for the species are set as convective flux. This ensures that all the mass transport through that boundary is convection dominated and there is no mass flux due to diffusion, since the normal components of the fluxes are zero. At the outlet of the gas flow channels, the pressure is set as the desired electrode pressure.

2.4.3. Boundary conditions for potential equations

At the anode channel/gas diffuser layer interface, the electronic potential is set to zero,

$$\Phi_s = 0 \quad (17)$$

and at the cathode channel/gas diffuser layer interface the current density boundary condition is adopted. The current density boundary condition was first employed by Meng and Wang [35], which enabled them to study the effect of electron transport on current density distribution and cell performance under prescribed current density.

$$-n \cdot (\sigma_s \nabla \Phi_s) = -I_{\text{avg}} \quad (18)$$

Table 2

Fuel cell geometries and operating conditions.

Parameter	Symbol	Value
Channel length	L_{ch}	2.5×10^{-2} m
Channel width	W_{ch}	5×10^{-4} m
Gas diffusion layer thickness	t_{gdl}	1.5×10^{-4} m
Membrane thickness	t_{m}	5.1×10^{-5} m
Cell temperature	T	333 K
Pressure	P	1.5 atm
Anode stoichiometry	ζ_a	1.5

2.4.4. Wall

No-slip and impermeable velocity conditions and no flux conditions are adopted.

$$\vec{u} = 0, \quad \frac{\partial c_k}{\partial n} = 0, \quad \frac{\partial p}{\partial n} = 0 \quad (19)$$

2.5. Numerical procedure

The time-dependent conservation equations were discretized by the finite element method and solved by Femlab software. Stringent numerical tests were conducted to achieve the mesh size and time step independence for the numerical solutions. It was shown that the calculation conducted on a mesh size of 4250 elements with first time interval $\Delta t = 0.1$ s was satisfactory, and these choices were used in this work to understand the transient process of PEMFC. Due to the memory and time requirements for the iteration process, the Femlab software was run on Dell Precision workstation (Intel Xeon 3.06 GHz, 1.5 GB SDRAM). It took about 850 s to complete each time-dependent simulation. Cell geometrical parameters and operating conditions are listed in Table 2. The physical and transport properties as well as the electrochemical kinetics parameters used in the present work are summarized in Table 3.

3. Experiment setup

3.1. Experiment system

A single PEMFC with an active surface area of 5 cm^2 was used to investigate the cell voltage response under a transient air flow and load change. The MEA consisted of a Nafion 212 membrane in combination with gas diffusion electrode (GDE) having a platinum loading of 0.4 mg cm^{-2} . In the preparation of the GDE, carbon paper from Toray, 40 wt. % Pt/C from E-TEK, PTFE suspension and Nafion® solution (Dupont, USA) were used. The MEA was pressed at 140°C for 120 s at a pressure of 1 MPa, and was positioned between two graphite plates which were tightened by bolts and nuts between two silver-plated metal plates. The graphite plates were grooved with parallel gas channels.

Hydrogen at the anode and air at the cathode were used as reactant gases and were humidified by passing each gas stream through a bubble type external humidifier. The flow rates of hydrogen and air were regulated by two mass flow controllers (Sensirion, Switzerland), the response time of which was less than 150 ms. The relative humidity of the reactant gases was controlled by adjusting the humidifier temperature which could be controlled by a LabVIEW-based program. The PEMFC was connected to a KFM 2030 (Kikusui, Japan) Electronic Load to measure the voltage and current. All important parameters during the PEMFC operation, i.e., cell potential, current, temperature, pressure and gas flow rates were controlled and collected by the aforementioned program. The PEMFC was preconditioned by operating with fully humidified hydrogen and air at 60°C and 0.05 MPa (gauge pressure) for 8 h.

Table 3
Physical and transport properties.

Property	Value	Reference
Viscosity of anode gas, μ_a	1.544×10^{-5} Pa s	[27]
Viscosity of cathode gas, μ_c	1.230×10^{-5} Pa s	[27]
$D_{H_2-H_2O}$ in anode gas channel	9.399×10^{-5} m ² s ⁻¹	[28–29]
$D_{O_2-H_2O}$ in cathode gas channel	2.883×10^{-5} m ² s ⁻¹	[28–29]
$D_{O_2-N_2}$ in cathode gas channel	2.422×10^{-5} m ² s ⁻¹	[28–29]
$D_{H_2O-N_2}$ in cathode gas channel	2.624×10^{-5} m ² s ⁻¹	[28–29]
$D_{H_2-H_2O}^{eff}$ in anode GDL	4.368×10^{-5} m ² s ⁻¹	[30]
$D_{O_2-H_2O}^{eff}$ in cathode GDL	1.340×10^{-5} m ² s ⁻¹	[30]
$D_{O_2-N_2}^{eff}$ in cathode GDL	1.126×10^{-5} m ² s ⁻¹	[30]
$D_{H_2O-N_2}^{eff}$ in cathode GDL	1.220×10^{-5} m ² s ⁻¹	[30]
Permeability of anode/cathode gas diffusion electrode, k	1.0×10^{-12} m ²	[31]
Porosity of anode/cathode gas diffusion electrode, ε_{GDE}	0.6	[35]
Anode exchange current density, $ai_{a,0}$	1×10^5 A m ⁻²	Estimated
Cathode exchange current density, $ai_{c,0}$	140 A m ⁻²	Estimated
Anode charge transfer coefficient for anode reaction, θ_a^a	0.5	[32]
Cathode charge transfer coefficient for anode reaction, θ_c^a	0.5	[32]
Anode charge transfer coefficient for cathode reaction, θ_a^c	0.5	[32]
Cathode charge transfer coefficient for cathode reaction, θ_c^c	0.5	[29]
Electrode conductivity, σ_s	570 S m ⁻¹	[33]
Reference hydrogen concentration, $c_{H_2,ref}$	40 mol m ⁻³	[20]
Reference oxygen concentration, $c_{O_2,ref}$	40 mol m ⁻³	[20]
Dry membrane density, ρ_{dry}	1980 kg m ⁻³	[34]
Equivalent weight of electrolyte in membrane, EW	1.1 kg mol ⁻¹	[34]

3.2. Experiment procedure

Since the aim of this study is to investigate the effect of variable air inlet flow rate on the cell potential transient response during the load change of the PEMFC, the anode inlet velocity was controlled at a fixed flow rate of 30 ml min⁻¹ (corresponding to an anode stoichiometry of 1.5 at 5000 A m⁻²). Using the parabolic pattern [36] for reference, the air flow rate changing in a parabolic form from 22 to 110 ml min⁻¹ (corresponding to a cathode stoichiometry of 2.5 at 5000 A m⁻²) in 1 s, 2 s and 4 s were set in our experiment during the load change from 0.05 to 2.5 A in 0.2 s. An abrupt air flow rate change has a potty effect on the relative humidity of the air, because the top of the bubble type external humidifier has enough space to buffer the impact of changes in the air flow rate. Therefore, the relative humidity change of the air could be neglected. Finally, the inlet flow rates of the anode/cathode remained constant at 30/110 ml min⁻¹. In order to study the effect of relative humidity on the cell potential transient response, different levels of relative humidity of hydrogen and air such as 100% and 62% were performed.

4. Results and discussions

4.1. Experimental results

The experimentally measured cell potential transient responses to a variable cathode flow rate during load change are shown in Fig. 2. It is clearly seen that the cell potential underwent an undershoot behavior under transient air flow and load change, and the magnitude of cell potential undershoot was affected by the air flow rate change rate. The lower the change rate, the greater the cell potential undershoots. For the cases at RH = 100%, when the air flow rate had changed from 22 to 110 ml min⁻¹ in 1/2/4 s, the corresponding minimum value of cell potential was 0.55/0.54/0.50 V, respectively. For different relative humidity, the magnitude of cell potential undershoots increased as the relative humidity decreased. For the cases of air flow rate changing from 22 to 110 ml min⁻¹ in 1 s, the cell potential reached minimum value of 0.55/0.48 V at RH = 100%/62%, respectively. It took about 20 s for the PEMFC to reach a new steady state. The steady state cell potential also decreased as the relative humidity was decreasing.

The steady state cell potentials for RH = 100%/62% were 0.62/0.58 V, respectively.

4.2. Model validation

To verify the model validity, we have studied the transient response of PEMFC by a mathematic model. For this purpose, we have imposed the current density to change from 100 to 5000 A m⁻² (corresponding to total current from 0.05 to 2.5 A) in 0.2 s, and the air inlet velocity to change in parabolic pattern within 1 and 4 s for the numerical simulation, as shown in Fig. 3. In this figure, the air flow rate changes in the experiments are compared with the model boundary conditions. It can be clearly seen that the air flow rate changes in the experiment agree well with those in the model boundary conditions. The base case is the cathode flow rate changing in 1 s in parabolic pattern and current density changing in 0.2 s under fully humidified.

Comparison of the results between the simulation and experimental data were made in Fig. 4. It is apparent that cell potential transient responses predicted by the model are in accord with the

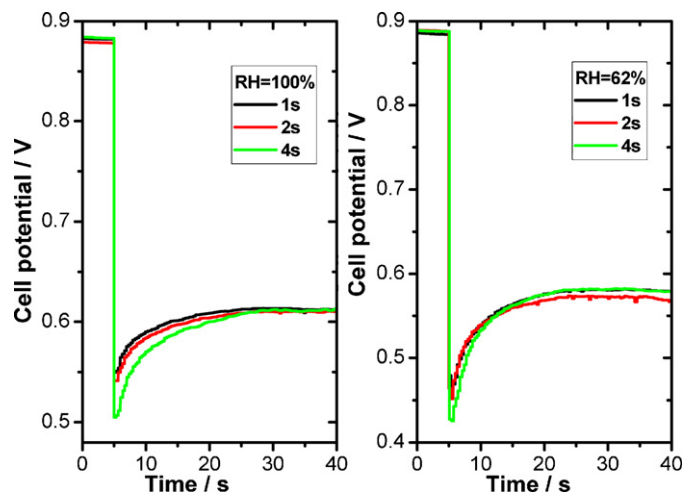


Fig. 2. Experiment results of cell potential transient response at different relative humidities.

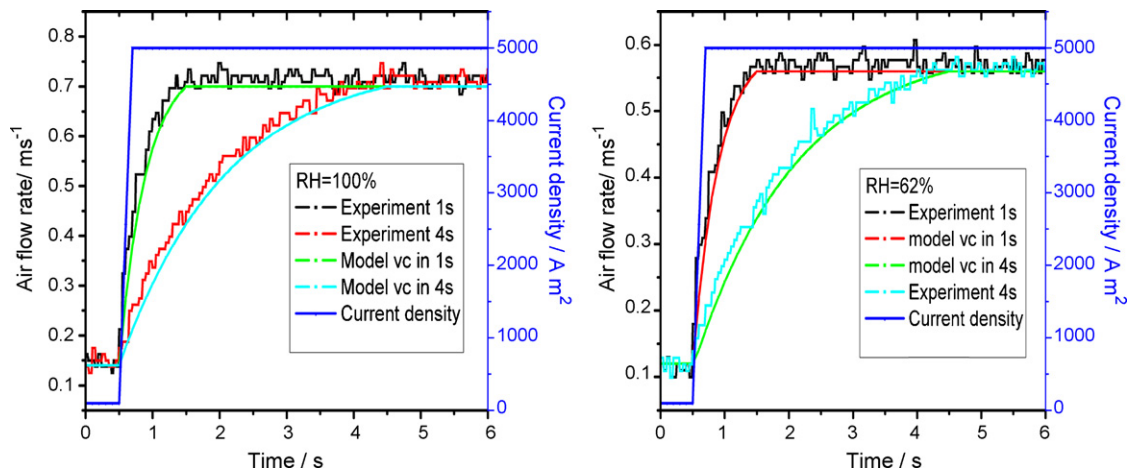


Fig. 3. Change with time of average current density and cathode inlet velocity.

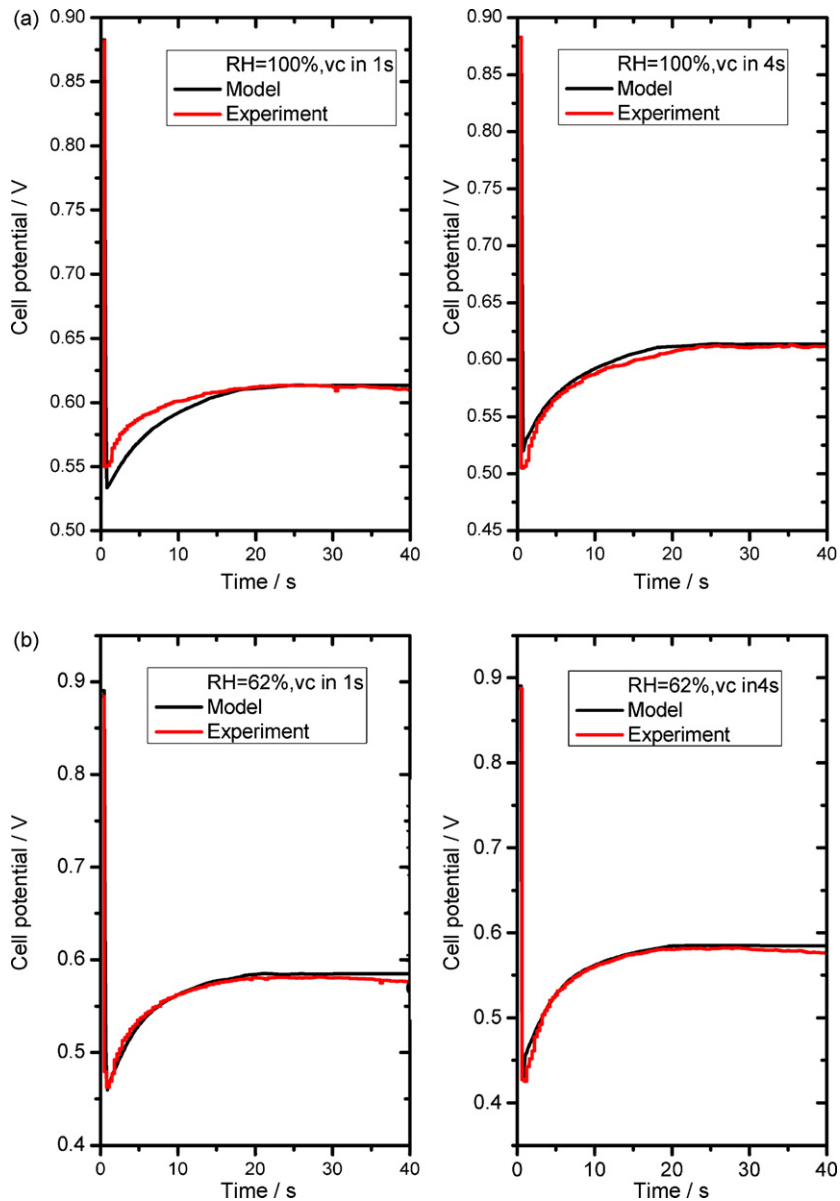


Fig. 4. Comparison of predicted and measured cell potential responses: (a) RH = 100%; (b) RH = 62%.

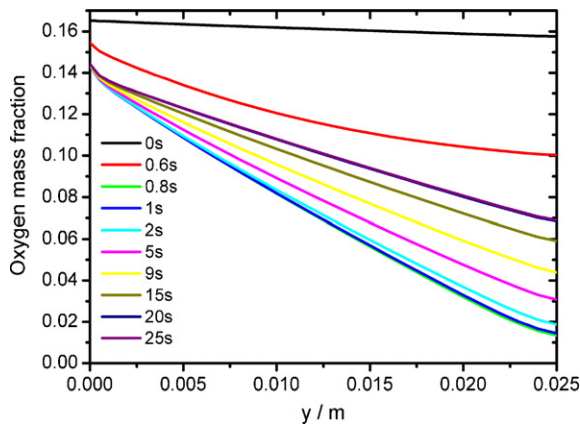


Fig. 5. Local oxygen mass fraction distribution on the cathode catalyst layer along the channel direction for base case.

experiment results at RH = 100% and RH = 62%. These validations have served to establish our confidence in the ability of the model to predict accurately the transient response of the test cell potential under transient air flow and load change of PEM fuel cell, thus rendering the possibility of using this model as a means for the study of the effect of the dynamic change in the membrane water content on the cell performance.

4.3. The effect of reactant starvation on the cell potential response

The instantaneous decrease in voltage was a result of increased activation and ohmic polarization. The activation polarization is mainly caused by the reactant starvation under transient air flow and load change, while the ohmic polarization is mainly related to the membrane resistance, which depends on membrane water content.

The local oxygen mass fraction at different time for the base case is shown in Fig. 5. In this figure, the top curve gives the initial oxygen mass fraction distribution, with an average current density value of 100 A m^{-2} . And the lower nine curves give the oxygen mass fraction distribution after the loading, with an average of 5000 A m^{-2} . By comparing the ten curves, the oxygen mass fraction at 0.8 s is the lowest downstream along the channel direction, resulting in the maximum cathode activation overpotential.

In order to illustrate the importance of the membrane water transport on cell potential, models considering with and without membrane water transport under a transient/constant air flow rate during load change were calculated. In the model without water transport equation, the membrane electrical conductivity was assumed to be constant at 0.1 S cm^{-1} [37]. The predicted cell potential responses with and without membrane water transport under RH = 62% are shown in Fig. 6. It can be seen that the response time under a constant air flow rate of 110 ml min^{-1} is about 12 s with membrane water transport, and no undershoot phenomena is observed in the case that has no membrane water transport. Under an air flow rate change of 1 s during the load change, the response time is about 1 s for the case of no membrane water transport, while about 20 s when there is membrane water transport. Based on these comparisons, it is concluded that the water transport across the membrane makes a great contribution to the cell dynamic behavior, which can also be verified by the comparison in time constants. Due to the fact that time constant is 10 s for membrane hydration, and 0.01 s for the gas to penetrate the GDL, water transport plays a dominant role on the response time [16,18,38].

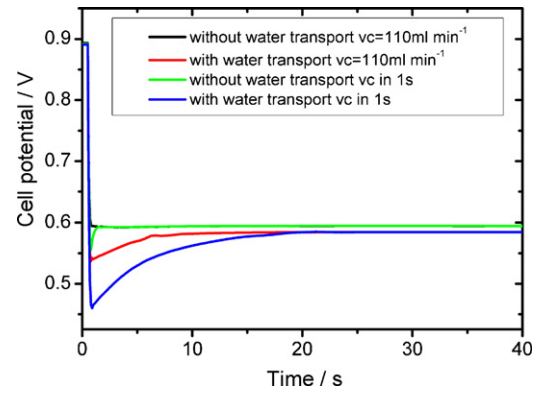


Fig. 6. Predicted cell potential response with and without membrane water transport under transient/constant air flow rate during load change at RH = 62%.

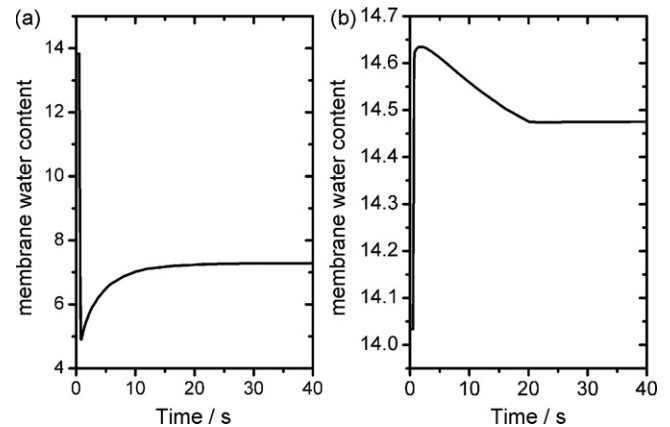


Fig. 7. The electrode/membrane interface water content transient response for RH = 100% (base case) (a) anode/membrane interface and (b) cathode/membrane interface.

4.4. The effect of relative humidity on the water content transient response

In this section, the effect of relative humidity on the water dynamic transport was investigated and the effect of water transport on cell potential response was also evaluated. Figs. 7 and 8 give the electrode/membrane interface water content transient response to variable cathode flow rate during the load change at RH = 100% and RH = 62%, respectively. When the current density was increased sharply, water molecules due to electro-osmotic

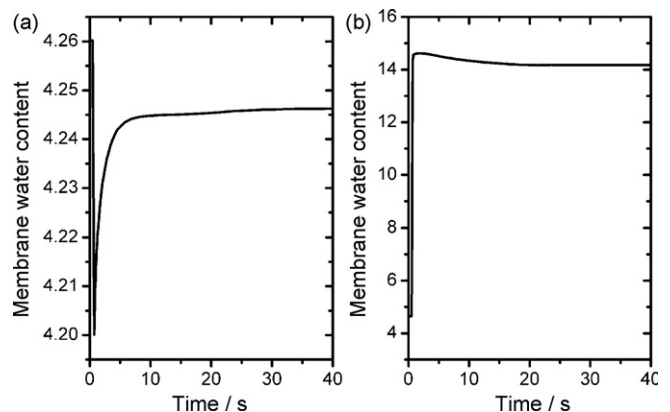


Fig. 8. The electrode/membrane interface water content transient response for RH = 62% (cathode flow rate changing in 1 s) (a) anode/membrane interface and (b) cathode/membrane interface.

drives also increased, which caused a decrease of the water content in the membrane adherent to the anode side. The anode/membrane interface water content reached the lowest value around 0.3 s after the load change, leading to the cell minimum potential shown in Fig. 5.

At the same time, more water was generated at the cathode catalyst layer, which increased proportionally to the current density jump. As time went on, the water concentration gradient between anode and cathode became larger, so that water would diffuse from the cathode to the anode. Due to this back-diffusion, the anode/membrane interface began to be rehydrated. The above phenomena can be clearly explained by Figs. 7 and 8 with different relative humidities. At RH = 100%, the initial water content at the anode/membrane interface was relatively high, its value was about 14. But at RH = 62%, the initial water content was about 4.3. This was due to the difference of inlet gas relative humidity. It took about 20 s for the water to establish a new equilibrium under the fully humidified condition, but it was nearly 30 s for RH = 62%. At a low humidity, water accumulation needed more time to reach a new equilibrium. The diffusive time-scale associated with the water transfer in the membrane has been investigated in detail elsewhere [16,38].

When the cell had reached a new steady state, the water content at the cathode/membrane interface was around 14. But at the anode/membrane interface, the water content was 7.3 at RH = 100%, while for RH = 62% it was 4.2. This resulted in a high membrane resistance and a lower potential value at RH = 62% at the steady state. Therefore, water redistribution in the PEMFC was controlled by the dynamic balance between electro-osmotic drag and back-diffusion in the proton exchange membrane, and the dynamic behavior of the PEMFC was critically dependent on the water transport in the proton exchange membrane.

5. Conclusions

In this paper, experimental and modeling investigations were carried out to study the effect of change in membrane water content on cell potential under transient air flow and load change of the PEMFC. Charge conservation equations were added to our previous two-dimensional isothermal dynamic model. The validity of the present model was confirmed by the comparison of the cell potential transient responses between the model predictions and the experiment results. Based on the model, the effect of relative humidity on the water dynamic transport and the effect of water transport on cell potential response were investigated.

The prediction results showed that the undershoot behavior in cell potential could be observed under transient air flow and load change conditions, and the magnitude of cell potential undershoot was affected by the change in air flow rate and the relative humidity. This was mainly due to the transient transfer of water in the proton exchange membrane, leading to the occurring of the differences in membrane resistance, and thus also in the cell potential. It was also found from the numerical prediction that the time scale for the cell potential to reach its steady state was about 20 s, in

agreement with experiment results. It was suggested that water redistribution in the PEMFC was controlled by the dynamic balance between electro-osmotic drag and back-diffusion in the proton exchange membrane, and the dynamic behavior of the PEMFC operation was critically dependent on the water transport in the proton exchange membrane.

Acknowledgements

This work was financially supported by the National High Technology Research and Development Program of China (863 Program No. 2007AA05Z131) and the National Natural Science Foundation of China (No. 20206030).

References

- [1] T. Murahashi, M. Naiki, E. Nishiyama, J. Power Sources 162 (2006) 1130–1136.
- [2] T.E. Springer, T.A. Zawodzinski, S. Gottesfeld, J. Electrochem. Soc. 138 (8) (1991) 2334–2342.
- [3] T.A. Zawodzinski, C. Derouin, S. Radzinski, R.J. Sherman, V.T. Smith, T.E. Springer, S. Gottesfeld, J. Electrochem. Soc. 140 (4) (1993) 1041–1047.
- [4] J.T. Hinatsu, M. Mizuhata, H. Takenaka, J. Electrochem. Soc. 141 (1994) 1493–1497.
- [5] G.J.M. Janssen, M.L.J. Overvelde, J. Power Sources 101 (2001) 117–125.
- [6] A. Husar, A. Higier, H.T. Liu, J. Power Sources 183 (2008) 240–246.
- [7] D.M. Bernardi, M.W. Verbrugge, AIChE J. 37 (1991) 1151–1163.
- [8] D.M. Bernardi, M.W. Verbrugge, J. Electrochem. Soc. 139 (1992) 2477–2491.
- [9] T. Okada, G. Xie, Y. Tanabe, J. Electroanal. Chem. 413 (1996) 49–65.
- [10] T. Okada, S. Møller-Holst, O. Gorseth, S. Kjelstrup, J. Electroanal. Chem. 442 (1998) 137–145.
- [11] T. Okada, J. Electroanal. Chem. 465 (1999) 1–17.
- [12] T. Okada, J. Electroanal. Chem. 465 (1999) 18–29.
- [13] F. Chen, M. Chang, C. Fang, J. Power Sources 164 (2007) 649–658.
- [14] M. Hsing, P. Futerko, Chem. Eng. Sci. 55 (2000) 4209–4218.
- [15] S. Um, C.Y. Wang, K.S. Chen, J. Electrochem. Soc. 147 (2000) 4485–4493.
- [16] Y. Wang, C.Y. Wang, Electrochim. Acta 50 (2005) 1307–1315.
- [17] Y. Wang, C.Y. Wang, Electrochim. Acta 51 (2006) 3924–3933.
- [18] H. Wu, P. Berg, X.G. Li, J. Power Sources 165 (2007) 232–243.
- [19] G. Hu, J. Fan, J. Power Sources 165 (2007) 171–184.
- [20] S.G. Qu, X.J. Li, M. Hou, Z.G. Shao, B.L. Yi, J. Power Sources 185 (2008) 302–310.
- [21] A.J. Bard, L.R. Faulkner, Electrochemical Methods, Wiley, New York, 1980.
- [22] A. Parthasarathy, S. Srinivasan, A.J. Appleby, J. Electrochem. Soc. 139 (1992) 2530–2537.
- [23] V. Gurau, H.T. Liu, S. Kakac, AIChE J. 44 (11) (1998) 2410–2422.
- [24] J. Fimrite, B. Carnes, H. Struchtrup, N. Djilali, J. Electrochem. Soc. 152 (2005) A1815–A1823.
- [25] P. Choi, N.H. Jalani, P. Datta, J. Electrochem. Soc. 152 (2005) E123–E130.
- [26] L. Pisani, M. Valentin, D.H. Hofmann, L.N. Kuleshova, B. D'Aguzzo, Solid State Ionics 179 (2008) 465–476.
- [27] R.C. Reid, J.M. Prausnitz, B.E. Poling, The Properties of Gases and Liquids, 4th ed., McGraw-Hill, New York, 1987.
- [28] R.B. Bird, W.E. Stewart, E.N. Lightfoot, Transport Phenomena, 2nd ed., Wiley, New York, 2002.
- [29] S. Yi, T.V. Nguyen, J. Electrochem. Soc. 146 (1999) 38–45.
- [30] S. Yi, T.V. Nguyen, J. Electrochem. Soc. 145 (1998) 1149–1159.
- [31] W. He, J.S. Yi, T.V. Nguyen, AIChE J. 46 (10) (2000) 2053–2064.
- [32] H. Ju, H. Meng, C.Y. Wang, Int. J. Heat Mass Transfer 48 (2005) 1303–1315.
- [33] P.T. Nguyen, T. Berning, N. Djilali, J. Power Sources 130 (2004) 14–157.
- [34] H. Meng, C.Y. Wang, Chem. Eng. Sci. 59 (2004) 3331–3343.
- [35] H. Meng, C.Y. Wang, Fuel Cells 5 (2005) 455–462.
- [36] M. Tekin, D. Hissel, M.-C. Pera, J.-M. Kauffman, J. Power Sources 156 (2006) 57–63.
- [37] E. I. du Pont de Nemours and Company, <http://www.dupont.com>.
- [38] H. Wu, X.G. Li, P. Berg, Int. J. Hydrogen Energy 32 (2007) 2022–2031.